Investigation of GaN-on-GaN vertical p-n diode with regrown p-GaN by metalorganic chemical vapor deposition

Kai Fu, Houqiang Fu, Hanxiao Liu, Shanthan Reddy Alugubelli, Tsung-Han Yang, Xuanqi Huang, Hong Chen, Izak Baranowski, Jossue Montes, Fernando A. Ponce, and Yuji Zhao

Citation: Appl. Phys. Lett. **113**, 233502 (2018); doi: 10.1063/1.5052479
View online: https://doi.org/10.1063/1.5052479
View Table of Contents: http://aip.scitation.org/toc/apl/113/23
Published by the American Institute of Physics

Investigation of GaN-on-GaN vertical *p-n* diode with regrown *p*-GaN by metalorganic chemical vapor deposition

Kai Fu,[1] Houqiang Fu,[1] Hanxiao Liu,[2] Shanthan Reddy Alugubelli,[2] Tsung-Han Yang,[1] Xuanqi Huang,[1] Hong Chen,[1] Izak Baranowski,[1] Jossue Montes,[1] Fernando A. Ponce,[2] and Yuji Zhao[1,a)]

[1]*School of Electrical, Computer and Energy Engineering, Arizona State University, Tempe, Arizona 85287, USA*

[2]*Department of Physics, Arizona State University, Tempe, Arizona 85287, USA*

(Received 18 August 2018; accepted 12 November 2018; published online 3 December 2018)

To mimic selective-area doping, p-GaN was regrown on an etched GaN surface on GaN substrates by metalorganic chemical vapor deposition. Vertical GaN-on-GaN *p-n* diodes were fabricated to investigate the effects of the etch-then-regrowth process on device performance. The crystal quality of the sample after each epitaxial step was characterized by X-ray diffraction, where the etch-then-regrowth process led to a very slight increase in edge dislocations. A regrowth interfacial layer was clearly shown by transmission electron microscopy. Strong electroluminescence was observed with three emission peaks at 2.2 eV, 2.8 eV, and 3.0 eV. The forward current density increased slightly with increasing temperature, while the reverse current density was almost temperature independent indicating tunneling as the reverse transport mechanism. This result is very similar to the reported Zener tunnel diode comprising a high doping profile at the junction interface. High levels of silicon and oxygen concentrations were observed at the regrowth interface with a distribution width of ~100 nm. This work provides valuable information on *p*-GaN regrowth and regrown GaN *p-n* diodes, which can serve as an important reference for developing selective doping for advanced GaN power electronics for high voltage and high power applications. *Published by AIP Publishing.*
https://doi.org/10.1063/1.5052479

Gallium nitride (GaN) power devices have become one of the most promising candidates for application in power electronic systems, offering remarkable improvements in energy conversion efficiency, switching frequency, and system volume.[1–3] As one of the most important fundamental building blocks of semiconductor electronic devices, *p–n* junctions, created by doping methods using ion implantation, diffusion of dopants, or epitaxy, are also of great importance in fabricating GaN power devices. However, although these doping methods are mature and commonly used in silicon (Si) and gallium arsenide (GaAs) devices, they are still difficult to implement for GaN, especially regarding *p*-type doping. It was found that GaN was not very resistant to ion beam disordering, and this problem became more severe at higher dose ion implantation.[4] Currently, it is still difficult to make good ohmic contacts on *p*-GaN by ion implantation.[5] For diffusion of dopants, the understanding of this process in GaN is still in its infancy. The high density of dislocations in GaN can strongly affect the effective diffusion penetration depth and surface dissociation becomes significant during high temperature annealing, which makes the diffusion method also difficult for GaN.[6] Epitaxy on GaN substrates may partly solve these issues due to the reduced dislocation density in the materials and doping during growth is still the most effective way to achieving well-controlled doping. Moreover, to fabricate high-performance GaN power devices and integrated circuits, selective-area doping is indispensable. However, a very few results have been reported on selective regrowth of GaN *p–n* diodes, and the physical mechanisms are still not clear,[7–10] especially on regrown p-GaN.[11] In this work, to mimic the selective-area doping, *p*-GaN was regrown on unintentionally doped (UID) GaN with an etched surface. The crystal quality, surface roughness, and regrowth interface were investigated. Vertical GaN-on-GaN *p–n* diodes were also fabricated to investigate the effects of the etch-then-regrowth process on device performance.

The samples were homoepitaxially grown by metalorganic chemical vapor deposition (MOCVD) on *c*-plane n^+-GaN free-standing substrates with a carrier concentration of $\sim 10^{18}\,cm^{-3}$ from Sumitomo Electric Industries Ltd. The growth temperature was ~1040 °C and hydrogen (H_2) was used as the carrier gas. 2-μm-thick UID-GaN epilayers were first grown on the substrate and then etched away 500 nm by an inductively coupled plasma (ICP). A 900-nm-thick *p*-GaN layer, with a Cp_2Mg flow rate of 0.15 μmol/min, was regrown on the etched surface. The activation of the regrown *p*-GaN was carried out by rapid thermal annealing at 700 °C for 20 min in a N_2 environment. The schematic structures and the regrowth process are shown in Fig. 1.

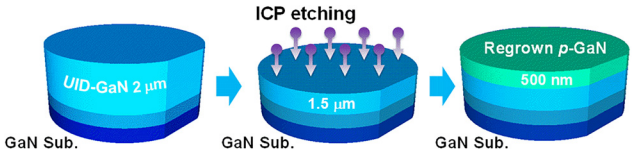

FIG. 1. Schematic structures and the regrowth process of the *p-n* junction on GaN substrates.

a)Email: yuji.zhao@asu.edu

Figure 2(a) shows the X-ray diffraction (XRD) omega rocking curves (RCs) for symmetric (002) and asymmetric (102) reflections of the regrown sample. The full-width-half-maxima (FWHMs) of the (002) and (102) planes are 57.0 arc sec and 27.0 arc sec, respectively. The dislocation density was estimated to be $3.5 \times 10^6\,\mathrm{cm}^{-2}$, which is much smaller than that of typical GaN-on-sapphire epilayers.[12] Figure 2(b) shows the FWHMs of (002) and (102) RCs of each step, including after the UID-GaN, after the etching and after the regrown *p*-GaN. A very slight increase in the (102) FWHM was observed, which indicates that edge dislocations were affected by the etch-then-regrowth process.[13,14] The root-mean-square (RMS) surface roughness of the regrown *p*-GaN was 0.66 nm, as measured by Bruker's Dimension atomic force microscopy (AFM) as shown in Fig. 2(c).

Vertical GaN-on-GaN *p–n* diodes were fabricated on the regrown sample by conventional processes. The sample was first cleaned in acetone and isopropyl alcohol under ultrasonication and then dipped in hydrochloric acid to remove native surface oxides before metal depositions. Pd/Ni/Au (10 nm/20 nm/50 nm) metal stacks were deposited by electron-beam evaporation for *p*-GaN ohmic contacts. Mesa isolations, with diameters ranging from 90 μm to 210 μm, were formed by the chlorine-based ICP dry etching with an ICP power of 400 W, a RF power of 70 W, and a pressure of 5 mTorr. Ti/Al/Ni/Au (20 nm/130 nm/50 nm/150 nm) metal stacks were also deposited by electron-beam evaporation for *n*-GaN ohmic contacts on the backside of the GaN substrate. Current-voltage (*I–V*) and capacitance-voltage (*C–V*) characteristics were measured using a Keithley 4200-SCS parameter analyzer and breakdown characteristics were measured with a Keithley 2410 sourcemeter.

During the forward *I–V* measurements, strong visible electroluminescence (EL) was observed, as shown in Fig. 3. Three EL peaks were found at 2.2 eV, 2.8 eV, and 3.0 eV, respectively, by fitting the EL spectrum using Gaussian equations. The schematic of transition processes for these peaks are shown in the inset of Fig. 3. The 2.2 eV peak was related to the well-known yellow luminescence in GaN, which is due to the capture of conduction band electrons by a deep acceptor level centered at 2.2 eV below the conduction band edge (CBE).[15] The 2.8 eV peak originated from the donor-acceptor pair (DAP) luminescence, i.e., the transition from a deep donor level (~0.4 eV below the CBE) to the Mg acceptor level, which is ~0.2 eV above the valence band

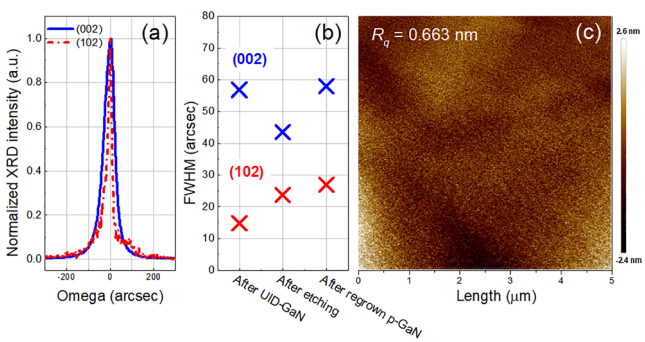

FIG. 2. (a) XRD omega rocking curves of (002) and (102) reflection of regrown *p*-GaN. (b) FWHMs after UID-GaN, after etching and after regrown *p*-GaN. (c) Surface morphology by AFM (5 μm × 5 μm).

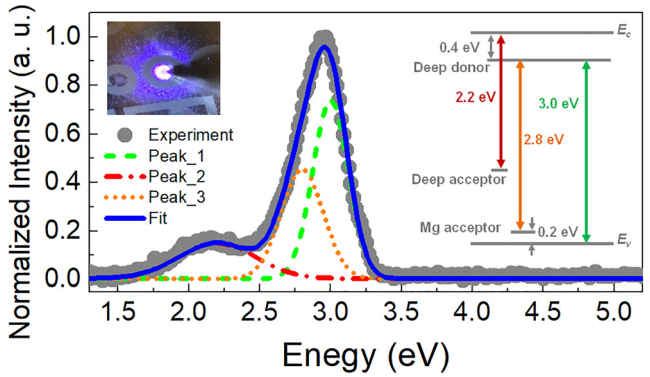

FIG. 3. EL spectrum of the regrown *p-n* junction and peaks by Gaussian fitting. The left inset shows the optical image of the light emission from the device under test. The right inset shows the energy levels in GaN.

edge (VBE).[16,17] The 3.0 eV peak was due to the transition from the deep donor to the VBE. The EL intensity of the regrown *p–n* diode is much lower than that of the as-grown diode indicating that the regrown interface contains many non-radiative recombination centers.

Figures 4(a) and 4(b) show temperature-dependent *I–V* curves of the regrown *p–n* diode. The turn-on voltage was 3.7 V, as extracted from linear extrapolation. It is a little larger than that of a typical as-grown GaN *p–n* diode, which could be due to the high recombination current, along with a large series resistance and minor shunt leakage currents.[11,18] The non-radiative recombination centers at the regrowth interface also lead to an abnormally larger ideality factor of over 5. The forward current density increased slightly with the increase in temperature, while the reverse current density was almost temperature independent indicating that tunneling is the dominant process in the reverse transport mechanism. This behavior is similar to the reported Zener tunnel

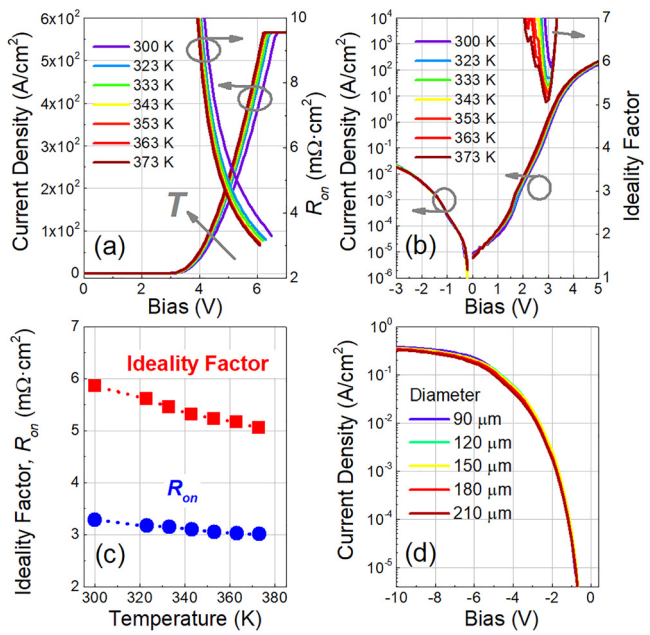

FIG. 4. (a) Temperature-dependent forward *I-V* curves and differential on-resistance in a linear scale. (b) *I-V* curves in a logarithmic scale and ideality factors as functions of temperature. (c) Summary of the ideality factor and differential on-resistance as functions of temperature. (d) Reverse leakage current densities vs. mesa diameters.

diode consisting of a p^+–n^+ junction.[19] The origin of the n^+-GaN layer in the regrown p–n junction could be attributed to the high Si concentration at the regrowth interface.[7,8] This will be investigated in detail in the following paragraph. We observed a slight decrease in the differential on-resistance with increasing temperature, as seen in Fig. 4(c). On-resistance is inversely proportional to electron mobility and carrier concentration. Since the electron mobility is reduced at high temperatures due to enhanced phonon scattering, this suggests that the increased carrier concentration caused the decrease in on-resistance at elevated temperatures.[20] This also led to the decrease in the ideality factor due to the changes in the slopes of forward temperature-dependent I–V curves. In Fig. 4(d), the reverse leakage currents were normalized by the mesa area with diameters ranging from 90 μm to 210 μm. It was found that the area-normalized leakage currents were almost the same at all voltages for different diameters, showing that the leakage current was proportional to the area of the devices. This indicates that the major leakage contributor was the bulk leakage current, instead of perimeter or sidewall leakage, where the leakage current is proportional to the diameter.

Figures 5(a)–5(c) show C–V curves of the regrown p–n diodes with various diameters at 10 kHz, 100 kHz, and 1 MHz, respectively. The frequency dispersion of the capacitance is indicative of defects distributed in the material. The area dispersion of the capacitance was also observed at 1 MHz, while this was not found at lower frequencies of 10 kHz and 100 kHz. This could result from the increased conductance (not shown here) or leakage due to the decreased impedance at high frequencies. Using a one-sided abrupt junction model, the relationship between capacitance, depletion width, and doping concentration can be given by[21]

$$C_d = \frac{\varepsilon_{GaN}}{W_d}, \tag{1}$$

$$\frac{d(1/C_d^2)}{dV} = \frac{-2}{q\varepsilon_{GaN}(N_D^+ - N_A^- + N_t)}, \tag{2}$$

where C_d is the depletion-layer capacitance per unit area, ε_{GaN} is the dielectric constant of GaN, W_d is the depletion width, N_D^+ is the ionized donor concentration, N_A^- is the ionized acceptor concentration, and N_t is the equivalent charge concentration of traps contributing to the frequency dispersion of the capacitance. Figure 6(a) shows the net charge concentration, $(N_D^+ - N_A^- + N_t)$, as a function of depletion width at 10 kHz and 100 kHz for the regrown p–n junction. There was a remarkably high positive charge concentration on the order of 10^{20}–10^{17} cm^{-3}, when the depletion width varied from 10 nm to 100 nm. This was attributed to the positively charged ionized donors at the interface with a distribution width of ~100 nm, which is consistent with the secondary-ion-mass spectrometry (SIMS) results shown in Fig. 7 and the reported results.[7,8] These donors were attributed to the high Si and oxygen (O) atoms at the regrowth interface. To further demonstrate this, another sample was also grown with a similar structure to aforementioned samples, except that a 275-nm-thick UID-GaN layer was regrown first as an insertion layer between p-GaN and etched UID-GaN. Figure 6(b) shows the net charge concentration as a function of depletion width at 10 kHz and 100 kHz for the regrown p–n junction with the UID-GaN insertion layer. The net charge concentration near p-GaN decreased by several orders of magnitude, since the regrowth interface was now located farther away from p-GaN. The high positive charge concentration was now moved to ~300 nm where the regrowth interface was included in the depletion region. These results show that the

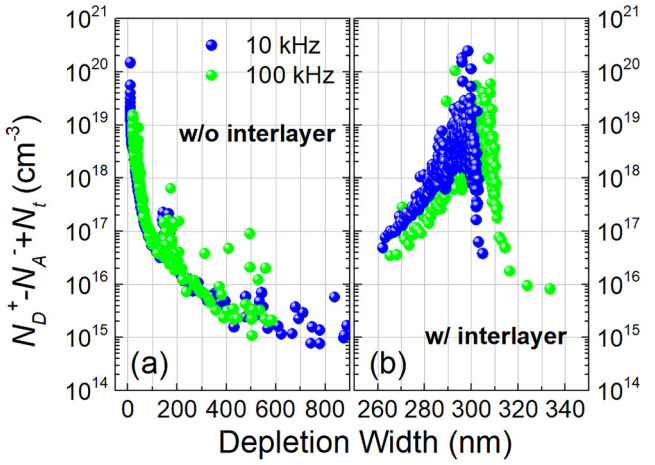

FIG. 6. Net charge concentration as a function of depletion width at 10 kHz and 100 kHz for the regrown p-n junction (a) without an inserting layer and (b) with an UID-GaN inserting layer.

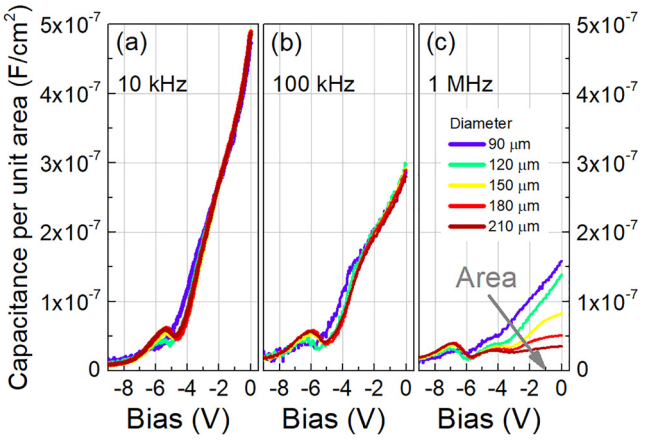

FIG. 5. C-V curves of regrown diodes with various diameters at (a) 10 kHz, (b) 100 kHz and (c) 1 MHz.

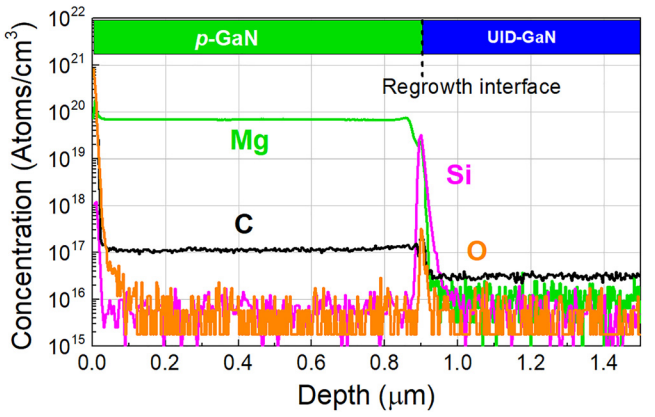

FIG. 7. SIMS profile of the regrown p-n junction showing high levels of Si and O atoms at the regrowth interface.

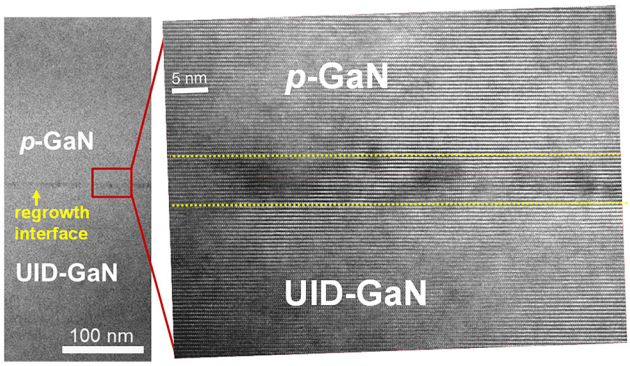

FIG. 8. TEM images of the regrown *p-n* junction.

etch-then-regrowth process introduced a high donor concentration layer at the regrowth interface.

Figure 8 shows transmission electron microscopy (TEM) images of the regrown *p–n* junction. A clear regrowth interfacial layer can be seen between the regrown *p*-GaN and UID-GaN. Due to the high Si-donor concentration at the regrowth interface, a thin n^+-GaN layer was formed right below the regrown *p*-GaN after the etch-then-regrowth process. This made the regrown *p–n* junction act like a Zener tunnel diode, which explains the tunneling dominated reverse leakage mechanism in Fig. 4(b). The enhanced local electric field created by high Si concentration at the interface also led to the premature breakdown of the junction and a low breakdown field of 1.04 MV/cm, which is much lower than the as-grown sample (∼3.4 MV/cm). This high donor concentration layer at the regrowth interface could be useful, such as for n^+-type doping, and should be eliminated in other cases since it enhances the local electric field.

In conclusion, GaN-on-GaN vertical *p–n* diodes with regrown *p*-GaN by MOCVD have been investigated. It was found that the etch-then-regrowth process could lead to a very slight increase in edge dislocations as revealed by XRD, and a clear regrowth interfacial layer by TEM. EL emission peaks for the regrown sample were related to the deep donor, the deep acceptor, and the Mg acceptor. *I–V* and *C–V* results suggested that the etch-then-regrowth process introduced a high donor concentration layer at the regrowth interface, as confirmed by the SMIS result. This made the regrown *p–n* diode act like a Zener tunnel diode, with temperature independent reverse leakage. This work can provide critical guidance for demonstrating advanced GaN power devices that involve the regrowth process.

This work was supported by the ARPA-E PNDIODES Program monitored by Dr. Isik Kizilyalli and partially supported by the NASA HOTTech Program grant number 80NSSC17K0768. We acknowledge the use of facilities within the Eyring Materials Center at Arizona State University. The device fabrication was performed at the Center for Solid State Electronics Research at Arizona State University. Access to the NanoFab was supported, in part, by NSF Contract No. ECCS-1542160.

[1]U. K. Mishra, L. Shen, T. E. Kazior, and W. Yi-Feng, Proc. IEEE **96**, 287 (2008).
[2]N. Ikeda, Y. Niiyama, H. Kambayashi, Y. Sato, T. Nomura, S. Kato, and S. Yoshida, Proc. IEEE **98**, 1151 (2010).
[3]H. Fu, X. Huang, H. Chen, Z. Lu, I. Baranowski, and Y. Zhao, Appl. Phys. Lett. **111**, 152102 (2017).
[4]S. Kucheyev, J. Williams, and S. Pearton, Mater. Sci. Eng. Rep. **33**, 51 (2001).
[5]Y. Zhang, Z. Liu, M. J. Tadjer, M. Sun, D. Piedra, C. Hatem, T. J. Anderson, L. E. Luna, A. Nath, A. D. Koehler, H. Okumura, J. Hu, X. Zhang, X. Gao, B. N. Feigelson, K. D. Hobart, and T. Palacios, IEEE Electron Device Lett. **38**, 1097 (2017).
[6]J. K. Sheu and G. C. Chi, J. Phys. Condens. Mater. **14**, R657 (2002).
[7]G. Koblmüller, R. M. Chu, A. Raman, U. K. Mishra, and J. S. Speck, J. Appl. Phys. **107**, 043527 (2010).
[8]H. Xing, S. P. DenBaars, and U. K. Mishra, J. Appl. Phys. **97**, 113703 (2005).
[9]R. D. Underwood, D. Kapolnek, B. P. Keller, S. P. Denbaars, and U. K. Mishra, Solid-State Electron. **41**, 243 (1997).
[10]A. Agarwal, O. Koksaldi, C. Gupta, S. Keller, and U. K. Mishra, Appl. Phys. Lett. **111**, 233507 (2017).
[11]Z. Hu, K. Nomoto, M. Qi, W. Li, M. Zhu, X. Gao, D. Jena, and H. G. Xing, IEEE Electron Device Lett. **38**, 1071 (2017).
[12]H. Q. Fu, X. Q. Huang, H. Chen, Z. J. Lu, X. D. Zhang, and Y. J. Zhao, IEEE Electron Device Lett. **38**, 763 (2017).
[13]B. Heying, X. H. Wu, S. Keller, Y. Li, D. Kapolnek, B. P. Keller, S. P. DenBaars, and J. S. Speck, Appl. Phys. Lett. **68**, 643 (1996).
[14]D. G. Zhao, D. S. Jiang, J. J. Zhu, Z. S. Liu, H. Wang, S. M. Zhang, Y. T. Wang, and H. Yang, Appl. Phys. Lett. **95**, 041901 (2009).
[15]I. Shalish, L. Kronik, G. Segal, Y. Rosenwaks, Y. Shapira, U. Tisch, and J. Salzman, Phys. Rev. B **59**, 9748 (1999).
[16]U. Kaufmann, M. Kunzer, M. Maier, H. Obloh, A. Ramakrishnan, B. Santic, and P. Schlotter, Appl. Phys. Lett. **72**, 1326 (1998).
[17]M. A. Reshchikov, G. C. Yi, and B. W. Wessels, Phys. Rev. B **59**, 13176 (1999).
[18]M. Qi, K. Nomoto, M. Zhu, Z. Hu, Y. Zhao, V. Protasenko, B. Song, X. Yan, G. Li, J. Verma, S. Bader, P. Fay, H. G. Xing, and D. Jena, Appl. Phys. Lett. **107**, 232101 (2015).
[19]X. Yan, W. Li, S. M. Islam, K. Pourang, H. Xing, P. Fay, and D. Jena, Appl. Phys. Lett. **107**, 163504 (2015).
[20]T. T. Mnatsakanov, M. E. Levinshtein, L. I. Pomortseva, S. N. Yurkov, G. S. Simin, and M. Asif Khan, Solid State Electron. **47**, 111 (2003).
[21]S. M. Sze and K. K. Ng, *Physics of Semiconductor Devices*, 3rd ed. (John Wiley & Sons, Inc., 2007).